

Crossed-beam reaction of carbon atoms with sulfur containing molecules.

I. Chemical dynamics of thioformyl ($\text{HCS}(X^2A')$) formation from reaction of $\text{C}(^3P_j)$ with hydrogen sulfide, $\text{H}_2\text{S}(X^1A_1)$

R. I. Kaiser,^{a)} C. Ochsenfeld,^{b)} M. Head-Gordon,^{c)} and Y. T. Lee^{d)}

Department of Chemistry, University of California, Berkeley, California 94720,

and Chemical Sciences Division, Lawrence Berkeley National Laboratory, Berkeley, California 94720

(Received 8 May 1998; accepted 27 October 1998)

The reaction between ground state carbon atoms, $\text{C}(^3P_j)$, and hydrogen sulfide, $\text{H}_2\text{S}(X^1A_1)$, was studied at four average collision energies between 16.7 and 42.8 kJ mol^{-1} using the crossed molecular beam technique. The reaction dynamics were deduced from time-of-flight spectra and from laboratory angular distributions combined with *ab initio* calculations. These data suggest that the reaction proceeds through an addition of $\text{C}(^3P_j)$ to the sulfur atom to form a triplet CSH_2 van der Waals complex. Successive H atom migration on the triplet or singlet surface forms a thiohydroxycarbene intermediate, HCSH , which decomposes through a tight exit transition state to $\text{HCS}(X^2A') + \text{H}(^2S_{1/2})$. At lower collision energies, a weak $\text{L-L}'$ coupling leads to isotropic center-of-mass angular distributions. As the collision energy rises, the angular distributions show increasing forward scattering thereby documenting that the reaction goes through an osculating HCSH complex. Identification of the HCS isomer under single collision conditions is a potential one-step pathway by which to form organo-sulfur molecules in interstellar environments during the collision of the comet Shoemaker-Levy 9 with Jupiter, and in combustion flames of sulfur containing fuels. © 1999 American Institute of Physics. [S0021-9606(99)01205-2]

I. INTRODUCTION

Although hydrogen, carbon, and sulfur are among the nine most abundant atoms in our universe,¹ the simplest neutral molecules containing these three atoms, thioformyl (HCS) and isothioformyl (HSC) radicals, have never been identified in extraterrestrial environments. However, since the ionized form of thioformyl, HCS^+ , and the oxygen homologues species $\text{HCOHCO}^+/\text{HOC}^+$ are well-known reactive intermediates in the interstellar medium, HCS and/or HSC are expected to be present at least in the interior of dense molecular clouds. Here, micrometer sized grain particles protect newly formed neutral molecules from destructive ionization and photodissociation through the external galactic ultraviolet radiation field.² The abundance of HCS/HSC and their local concentration profiles could yield important information on the organo-sulfur chemistry in these environments and help to understand the chemistry and mechanisms in order to synthesize astronomically observed cummulenes C_2S , C_3S , C_5S as well as the sulfur containing species CS , SiS , NS , SO , SO_2 , H_2S , COS , HNCS , CH_3SH , H_2CS , HCS^+ , and CS^+ .³ Even in our solar system, the sulfur chemistry is far from explained. Although the production of

H_3S^+ , HCS^+ , H_3CS^+ , and SO^+ in cometary comae⁴ is thought to involve ion-molecule reactions together with photochemistry, formation mechanisms of the H_2S , CS , and H_2CS parent molecules have not been identified. Likewise, the source of sulfur compounds CS , CS_2 , COS , and S_2 detected in the upper jovian atmosphere immediately after the impact of comet fragments of Shoemaker-Levy (SL9) into Jupiter is unknown.⁵ Here, shock-wave chemistry requires the formation of sulfur containing reaction mediates such as thioformaldehyde H_2CS and the thioformyl radical HCS to reproduce at least CS production rates after the impact. But even the formation mechanisms of these sulfur containing isomers need to be solved.

Even though the physical parameters in cold, molecular clouds and terrestrial combustion flames such as pressures and temperatures ($< 10^{-11}$ Torr and 10–30 K vs about 760 Torr and up to 5000 K) strongly differ, the potential HCS/HSC formation in both environments is expected to be closely related. Here, atomic carbon and hydrogen sulfide were observed in the interstellar medium as well as in combustion flames.^{6,7} $\text{C}(^3P_j)$ could react with H_2S via a carbon-hydrogen exchange to form HCS/HSC and atomic hydrogen in both environments. Although atomic oxygen is more abundant than carbon atoms in combustion flames, the reaction rate constant of the $\text{O}(^3P_j)/\text{H}_2\text{S}$ system is up to two orders of magnitude lower⁸ compared to $\text{C}(^3P_j)/\text{H}_2\text{S}$. This clearly eliminates the advantage of a larger oxygen concentration, and the title reaction might transform H_2S molecules into highly unstable HCS radicals. In hydrocarbon flames, HCS/HSC could decompose into H atoms as could reactive CS as well. CS might react further with four and five carbon

^{a)}Present address: Academia Sinica, Institute of Atomic and Molecular Sciences, 1, Sec. 4, Roosevelt Rd., Taipei 106, Taiwan, ROC and Dept. of Physics, Technical University Chemnitz-Zwickau, 09107 Chemnitz, Germany; electronic mail: kaiser@po.iams.sinica.edu.tw

^{b)}Electronic mail: chi@alcatraz.cchem.berkeley.edu

^{c)}Electronic mail: mhg@alcatraz.cchem.berkeley.edu

^{d)}Present address: Academia Sinica, Institute of Atomic and Molecular Sciences, 1, Sec. 4, Roosevelt Rd., Taipei 106, Taiwan, ROC; electronic mail: ytleee@gate.sinica.edu.tw

TABLE I. Experimental conditions and 1σ errors averaged over the experimental time: most probable velocity v_0 , speed ratio S , most probable relative collision energy, E_{coll} , center-of-mass angle, θ_{CM} , composition of the carbon beam, and flux factor $f_v = n(C) \times n(\text{H}_2\text{S}) \times v_r$ in relative units, with the number density of the i th reactant n_i and the relative velocity v_r .

Beam	v_0 (ms^{-1})	S	E_{coll} (kJ mol^{-1})	θ_{CM}	$C_1:C_2:C_3$	f_v
$\text{C}(^3P_j)/\text{Ne}$	1730 ± 21	3.2 ± 0.4	16.7 ± 0.5	55.0 ± 0.6	1:0.6:1.5	1.0
$\text{C}(^3P_j)/\text{Ne}$	2040 ± 26	4.1 ± 0.5	20.9 ± 0.6	45.8 ± 0.5	1:0.5:1.4	1.4 ± 0.6
$\text{C}(^3P_j)/\text{Ne}$	2680 ± 33	2.3 ± 0.3	34.9 ± 0.8	42.9 ± 0.4	1:0.2:0.4	6.2 ± 3.5
$\text{C}(^3P_j)/\text{He}$	2980 ± 50	2.5 ± 0.4	42.8 ± 1.3	38.3 ± 0.5	1:0.3:0.6	6.7 ± 3.7
H_2S	740–880	7.0–13.0

atoms containing hydrocarbon radicals to the thioheterocyclic compound⁹ and even sulfur containing polycyclic aromatic hydrocarbon molecules.

Due to the potential implications of the $\text{C}(^3P_j)/\text{H}_2\text{S}$ system in interstellar, planetary, and combustion chemistry, we investigate the energy dependent chemical dynamics of the reaction of atomic carbon, $\text{C}(^3P_j)$, with hydrogen sulfide, $\text{H}_2\text{S}(X^1A_1)$ under single collision conditions in crossed molecular beam experiments at four different collision energies between 16.7 and 42.8 kJ mol^{-1} . The product velocity and angular distributions measured combined with state-of-the-art *ab initio* calculations on the doublet HCS and triplet/singlet CH_2S surfaces identify the primary reaction channel(s) and obtain information on the elementary steps of the reaction.

II. EXPERIMENT AND DATA ANALYSES

The experiments were performed with a universal crossed molecular beam apparatus that is described in Ref. 10. A pulsed supersonic carbon beam was generated via laser ablation of graphite at 266 nm.¹¹ The 30 Hz, 40–45 mJ output of a Spectra Physics GCR-270-30 Nd:YAG laser is focused onto a rotating carbon rod, and ablated carbon atoms are seeded into neon or helium carrier gas released by a Proch-Trickl pulsed valve operating at 60 Hz and 80 μs pulses with 4 atm backing pressure. A four-slot chopper wheel selects a 9 μs segment of the carbon beam. Table I summarizes the experimental conditions. The pulsed hydrogen sulfide beam was held at 580 ± 5 Torr backing pressure and crossed the carbon beam at 90° in the interaction region of the scattering chamber. Time-of-flight spectra (TOF) of the products were detected in the plane of the beams using a rotatable quadrupole mass spectrometer with an electron-impact ionizer at different laboratory angles in 5.0° steps at $m/e = 45$ (HC^{32}S , hereafter HCS) and $m/e = 44$ (C^{32}S , hereafter CS).¹²

Information on the reaction dynamics was supplied by fitting the TOF spectra and the laboratory product angular distributions (LAB) using a forward-convolution routine described in Ref. 13. This approach initially guesses the angular flux distribution $T(\theta)$ and the translational energy flux distribution $P(E_T)$ in the center-of-mass (CM) system assuming mutual independence. TOF spectra and the laboratory angular distributions are then calculated from these

$T(\theta)$ and $P(E_T)$ convoluted over the apparatus functions to obtain simulations of the experimental data.

III. AB INITIO CALCULATIONS

All *ab initio* results presented in this article were computed at the CCSD(T) (single- and double-excitation coupled cluster with a perturbational estimate of triple excitations) level¹⁴ based on unrestricted Hartree-Fock (UHF) wave functions using pure spherical harmonic basis functions in the ACES II program package.¹⁵ The structures were fully optimized at the CCSD(T) level using triple zeta polarization (TZP) basis sets for H_2CS isomers and quadruple zeta double polarization (QZPP)¹⁶ for HCS and HSC. Vibrational frequencies within the harmonic approximation and zero-point energies were obtained in the same way. The relative energies for the H_2CS isomers and for HCS/HSC were calculated at the QZPP and QZ3P level (QZ triple polarization), respectively. We used Dunning's exponents for the polarization functions PP and 3P.¹⁷ The reaction energies were obtained at the CCSD(T)/QZPP level for the reaction of $\text{C}(^3P_j) + \text{H}_2\text{S} \rightarrow \text{H}_2\text{CS}$. For the reaction of $\text{C}(^3P_j) + \text{H}_2\text{S} \rightarrow \text{HCS/HSC} + \text{H}$, CCSD(T)/QZ3P single-point calculations at the CCSD(T)/QZPP structures were used. These reaction energies are estimated to be accurate to about 5–10 kJ mol^{-1} . The systematic *ab initio* investigations are described elsewhere,¹⁸ where methodical aspects, energies, energy differences, geometries, and vibrational frequencies are discussed in detail. Here, we focus on results essential to investigation of our experimental data. We would like to point out that none of the orbital considerations in this article are based on our *ab initio* calculations. These orbital correlations are qualitative, but useful models to explain our results.

IV. RESULTS

A. Reactive scattering signal

We observed the reactive scattering signal at $m/e = 45$, i.e., HCS/HSC; see Figs. 1–8 and Table II. TOF spectra were recorded at $m/e = 44$. (CS) as well, but they show shapes identical to the TOFs of HCS/HSC. This indicates that the energetically accessible channels 3 and 4 to form CS and $2\text{H}/\text{H}_2$ are closed in our experiments. No radiative association to any CH_2S isomers at $m/e = 46$ was observed. Finally, no higher masses were detected, demonstrating that carbon

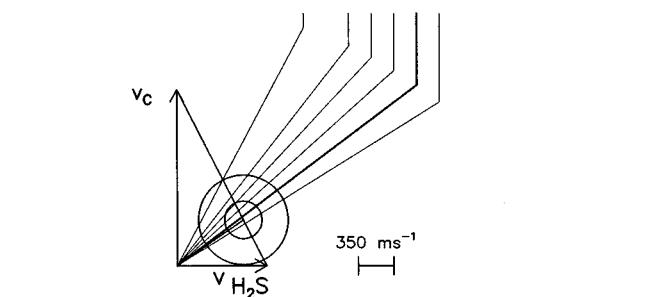
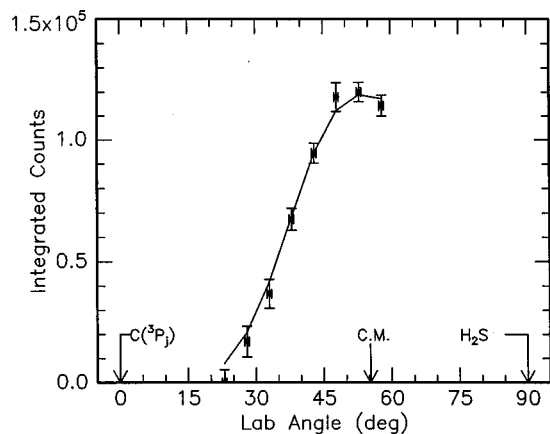


FIG. 1. Bottom: Newton diagram for the reaction $C(^3P_j) + H_2S(X^1A_1)$ at a collision energy of 16.7 kJ mol^{-1} . The circles stand for the maximum center-of-mass recoil velocity of different HCS (innercircle: HSC, outer-circle: HCS). Top: Laboratory angular distribution of the product channel at $m/e=45$. The circles and 1σ error bars indicate experimental data, and the solid lines the calculated distributions. C.M. designates the center-of-mass angle. The solid lines point to distinct laboratory angles whose TOFs are shown in Fig. 5.

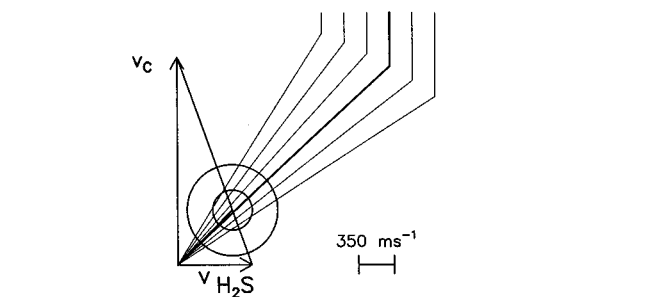
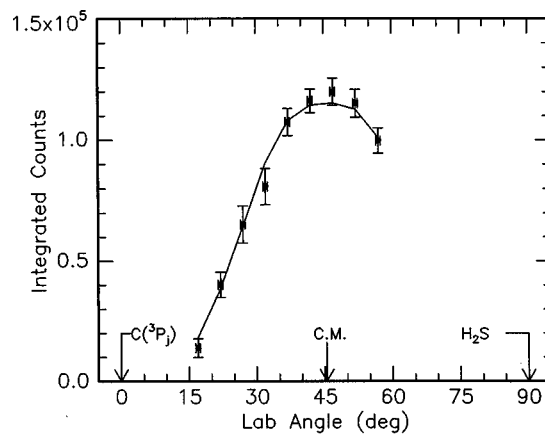


FIG. 2. Bottom: Newton diagram for the reaction $C(^3P_j) + H_2S(X^1A_1)$ at a collision energy of 20.9 kJ mol^{-1} . The circles stand for the maximum center-of-mass recoil velocity of different HCS (innercircle: HSC, outer-circle: HCS). Top: Laboratory angular distribution of the product channel at $m/e=45$. The circles and 1σ error bars indicate experimental data, and the solid lines the calculated distributions. C.M. designates the center-of-mass angle. The solid lines point to distinct laboratory angles whose TOFs are shown in Fig. 6.

clusters C_2 and C_3 do not contribute to the reactive scattering signal. This is quite a correlation with earlier studies of reactions of closed shell hydrocarbons with C, C_2 , and C_3 . The earlier investigations showed the absence of C_2 and C_3 reaction products.¹⁹

B. Laboratory angular distributions and time-of-flight spectra

The most probable Newton diagrams are displayed together with laboratory angular distributions at collision energies of 16.7, 20.9, 34.9, and 42.8 kJ mol^{-1} in Figs. 1–4. At lower collision energies of 16.7 and 20.9 kJ mol^{-1} , both distributions peak at 53° and 47° , close to the center-of-mass angles of 55.0° and 46.8° , respectively. Increasing the collision energies to 34.9 and 42.8 kJ mol^{-1} results in LAB distributions showing a preferred forward scattering with respect to the carbon beam, i.e., maxima at 33.0° and 30.0° versus CM angles of 42.9° and 38.3° . These data imply a reduced lifetime in a decomposing CH_2S complex with rising collision energy. In addition, all LAB distributions are very broad and extend up to 60° in the scattering plane. This indicates that the energy release into the translational degrees of freedom of the products is large. Based on this, the $P(E_T)$'s are expected to peak well away from zero translational energy (see Sec. IV C). If we compare these scattering

ranges with limiting circles corresponding to the maximum energy release of reactions 1 and 2 and assume all available energy channels into product translation, we find that at least the HCS isomer is formed at all collision energies.

C. Center-of-mass translational energy distributions, $P(E_T)$'s

Figure 9 shows the best fits of the translational energy distributions, $P(E_T)$'s, and angular distributions, $T(\theta)$, in the center-of-mass reference frame. We obtained best fits of the LAB distributions and TOF spectra with $P(E_T)$ extending to maximum translational energy releases E_{\max} of 205, 210, 220, and 235 kJ mol^{-1} at collision energies of 16.7, 20.9, 34.9, and 42.8 kJ mol^{-1} . Within the error limits of our experimental data, the high energy cutoffs can be extended by an additional 30–40 kJ mol^{-1} without having a significant effect on the fits. Comparing E_{\max} of our best fits with the sum of the exothermicity of reaction (1) plus the relative collision energies gives cutoffs at 200.6, 204.85, 218.8, and $226.7 \text{ kJ mol}^{-1}$, cf. Table I. The $165.6 \text{ kJ mol}^{-1}$ less stable HSC(X^2A') isomer can be excluded as a major contributor to our reactive scattering signal. In this case, high energy cutoffs at 35.0, 39.2, 53.2, and 61.1 kJ mol^{-1} are expected. Further, the most probable translational energy gives the order of magnitude of the exit barrier. Here, the $P(E_T)$'s peak

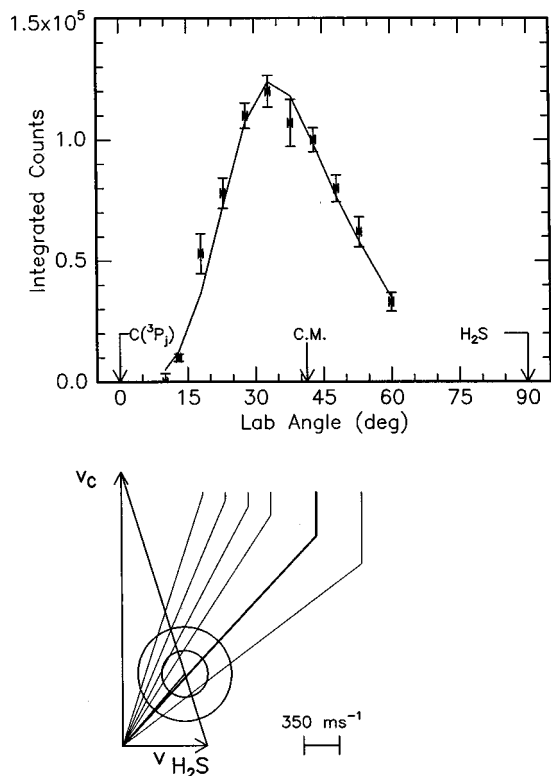


FIG. 3. Bottom: Newton diagram for the reaction $C(^3P_j) + H_2S(X^1A_1)$ at a collision energy of 34.9 kJ mol^{-1} . The circles stand for the maximum center-of-mass recoil velocity of different HCS (innercircle: HSC, outer-circle: HCS). Top: Laboratory angular distribution of the product channel at $m/e=45$. The circles and 1σ error bars indicate experimental data, and the solid lines the calculated distributions. C.M. designates the center-of-mass angle. The solid lines point to distinct laboratory angles whose TOFs are shown in Fig. 7.

at $44\text{--}53 \text{ kJ mol}^{-1}$ (both lower collision energies), increasing to about $61\text{--}72 \text{ kJ mol}^{-1}$ as the collision energy rises. The order of magnitude of the exit barrier suggests a tight exit transition state from the fragmenting CH_2S complex to the products. A loose transition state would have resulted in $P(E_T)$'s peaking close to zero translational energy. The repulsive energy release is further documented by the large fraction of available energy released into product translation, i.e., $38 \pm 2\%$ and $40 \pm 4\%$ at both lower and higher collision energies, respectively.

D. Center-of-mass angular distributions, $T(\theta)$ s

The shape of the center-of-mass angular flux distributions can be employed to collect additional information on the chemical dynamics of the reaction; cf. Fig. 9. At lower collision energies, both $T(\theta)$'s are weakly polarized and show isotropic distributions symmetric around $\pi/2$. This indicates that the decomposing CH_2S complex either has a lifetime longer than its rotational period τ_r , or that the exit transition state is "symmetric:" the CH_2S complex rotates and interconverts both H atoms through an n -fold symmetry axis. Hence the H atom could be ejected with equal probability to the CM angles θ and $\pi-\theta$ resulting in a symmetric distribution. In this case, the lifetime of the fragmenting complex cannot be determined. As the collision energy rises

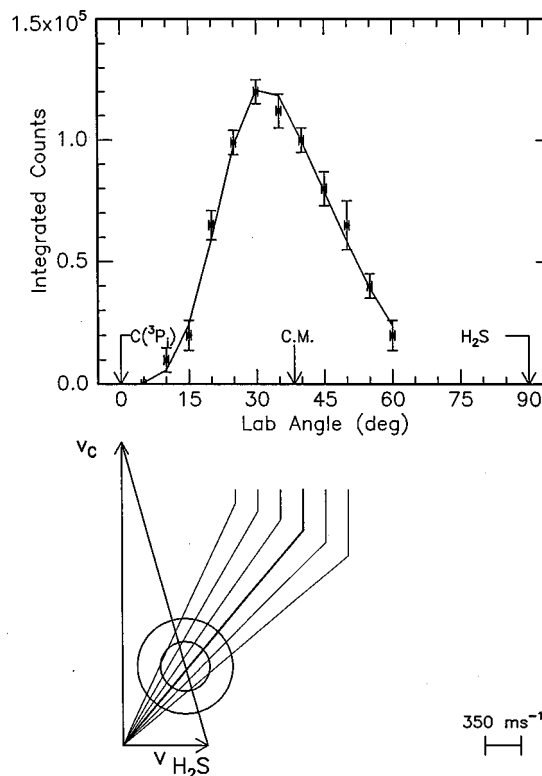


FIG. 4. Bottom: Newton diagram for the reaction $C(^3P_j) + H_2S(X^1A_1)$ at a collision energy of 42.8 kJ mol^{-1} . The circles stand for the maximum center-of-mass recoil velocity of different HCS (innercircle: HSC, outer-circle: HCS). Top: Laboratory angular distribution of the product channel at $m/e=45$. The circles and 1σ error bars indicate experimental data, and the solid lines the calculated distributions. C.M. designates the center-of-mass angle. The solid lines point to distinct laboratory angles whose TOFs are shown in Fig. 8.

to 34.9 and 42.8 kJ mol^{-1} , the $T(\theta)$'s depict an enhanced intensity at 0° compared to 180° of 2.8 ± 0.1 and 3.15 ± 0.15 within the experimental error limits, respectively. According to this trend it seems that there is indirect scattering dynamics through a complex formation and a reduced lifetime of the H_2CS complex with increasing collision energy (osculating complex). Based on this intensity ratio, we can use the rotational period as a clock to estimate the lifetime of the complex once the complex and its rotational axis are identified, see Secs. V C and V D. To account for the forward scattering found experimentally the carbon atom incorporated and the H atom leaving must be placed on opposite sides of the rotational axis.¹⁹ This helps us to identify or at least to narrow down the possible rotational axis(es).

The mild polarization of both $T(\theta)$'s at lower collision energies is the result of total angular momentum conservation and angular momentum disposal.²⁰ If we employ a classical treatment and neglect quantum mechanical effects, the total angular momentum \mathbf{J} is given by $\mathbf{J} = \mathbf{L} + \mathbf{j} = \mathbf{L}' + \mathbf{j}'$ with the initial and final orbital angular momenta \mathbf{L} and \mathbf{L}' perpendicular to the initial and final relative velocity vectors \mathbf{v} and \mathbf{v}' , and \mathbf{j} and \mathbf{j}' the rotational angular momenta of reactants and products. An upper limit of the impact parameter b_{\max} and hence L_{\max} can be calculated assuming that the reaction proceeds within orbiting limits and with unit effi-

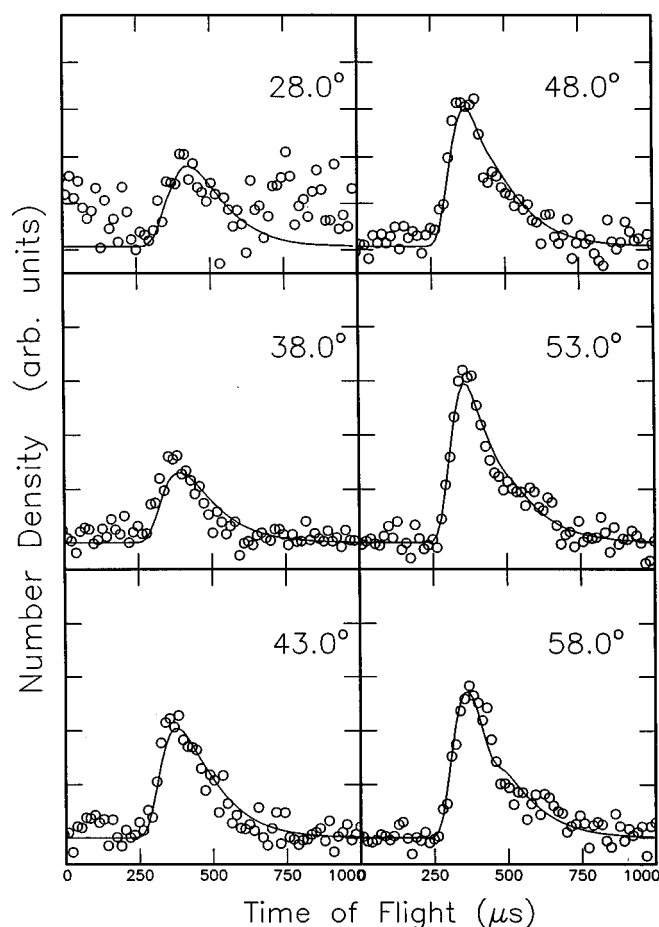


FIG. 5. Time-of-flight data at $m/e=45$ for distinct laboratory angles at a collision energy of 16.7 kJ mol^{-1} . The open circles represent experimental data, and the solid line the fit. The TOF spectra have been normalized to the relative intensity at each angle. The TOF at 28.0° is magnified.

ciency after barrier crossing; see Table III. Using the C_6 Lennard-Jones coefficient²¹ with the ionization potentials $E_{C(3P_j)} = 11.76 \text{ eV}$, $E_{\text{H}_2\text{S}} = 10.453 \text{ eV}$, and polarizabilities $\alpha_{C(3P_j)} = 1.76 \times 10^{-30} \text{ m}^3$, $\alpha_{\text{H}_2\text{S}} = 3.875 \times 10^{-30} \text{ m}^3$,⁸ b_{max} is calculated to $3.2\text{--}3.8 \text{ \AA}$, and the maximum orbital angular momentum to $139\text{--}102 \hbar$. Since H_2S is produced in a supersonic expansion, \mathbf{j} contributes less than 4% to the total angular momentum \mathbf{J} , hence $\mathbf{L} \approx \mathbf{J} = \mathbf{L}' + \mathbf{j}'$. The poor $T(\theta)$ polarization requires that \mathbf{L} and \mathbf{L}' must be uncoupled from $\mathbf{L} \gg \mathbf{L}'$, and a significant fraction of \mathbf{L} is expected to go into rotational excitation of the HCS product. Since the H atom emitted is very light compared to the HCS (1:45), the weak $\mathbf{L}\text{--}\mathbf{L}'$ correlation is a direct result of the ineffectiveness of the H atom to take away a substantial amount of orbital angular momentum.

E. Flux contour maps and total relative cross sections

The center-of-mass flux contour maps $I(\theta, E_T) \sim T(\theta) \times P(E_T)$ are displayed for all four collision energies in Figs. 10–13. As anticipated from the center-of-mass angular distributions, both distributions at lower collision energies show a forward-backward symmetric profile. A pronounced for-

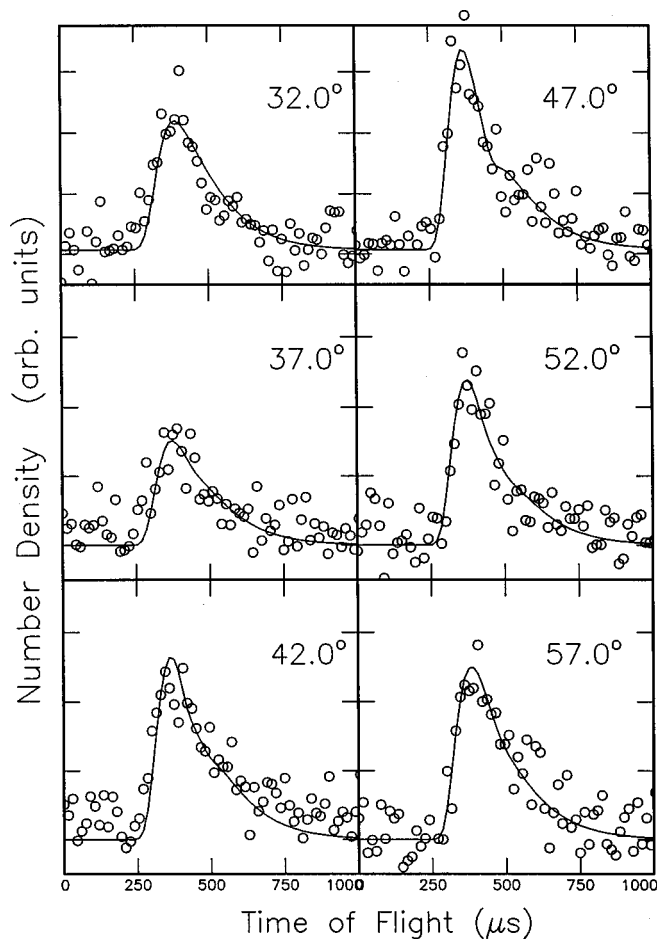


FIG. 6. Time-of-flight data at $m/e=45$ for distinct laboratory angles at a collision energy of 20.9 kJ mol^{-1} . The open circles represent experimental data, and the solid line the fit. The TOF spectra have been normalized to the relative intensity at each angle.

ward peaking is found as the collision energy rises to 34.9 and 42.8 kJ mol^{-1} . If we integrate this flux distribution and correct the reactant flux as well as the relative reactant velocity (cf. Table I), we find relative cross section ratios of $\sigma(16.7 \text{ kJ mol}^{-1})/\sigma(20.9 \text{ kJ mol}^{-1})/\sigma(34.9 \text{ kJ mol}^{-1})/\sigma(42.8 \text{ kJ mol}^{-1}) = 1.5 \pm 0.4/1.4 \pm 0.3/1.3 \pm 0.3/1.0$. Reactions of $C(3P_j)$ with unsaturated hydrocarbons studied earlier by our group depict a rising cross section within the orbiting limits as the collision energy dropped.²² However, the energy dependence of the title reaction is less pronounced. The orbiting model predicts an $E^{-1/3}$ energy dependence, i.e., $\sigma(16.7 \text{ kJ mol}^{-1})/\sigma(20.9 \text{ kJ mol}^{-1})/\sigma(34.9 \text{ kJ mol}^{-1})/\sigma(42.8 \text{ kJ mol}^{-1}) = 1.37/1.27/1.07/1.0$. Due to the large experimental errors, the expected strong energy dependence within orbiting limits cannot be confirmed experimentally.

V. DISCUSSION

A. The singlet/triplet CH_2S and doublet HCS *ab initio* potential energy surfaces

The singlet thioformaldehyde isomer $\{7\}$, H_2CS , (PES) is the global minimum on the CH_2S potential energy surface and is bound by $550.4 \text{ kJ mol}^{-1}$ with respect to the reactants (Table IV and Fig. 14). Our calculations suggest a C_{2v} sym-

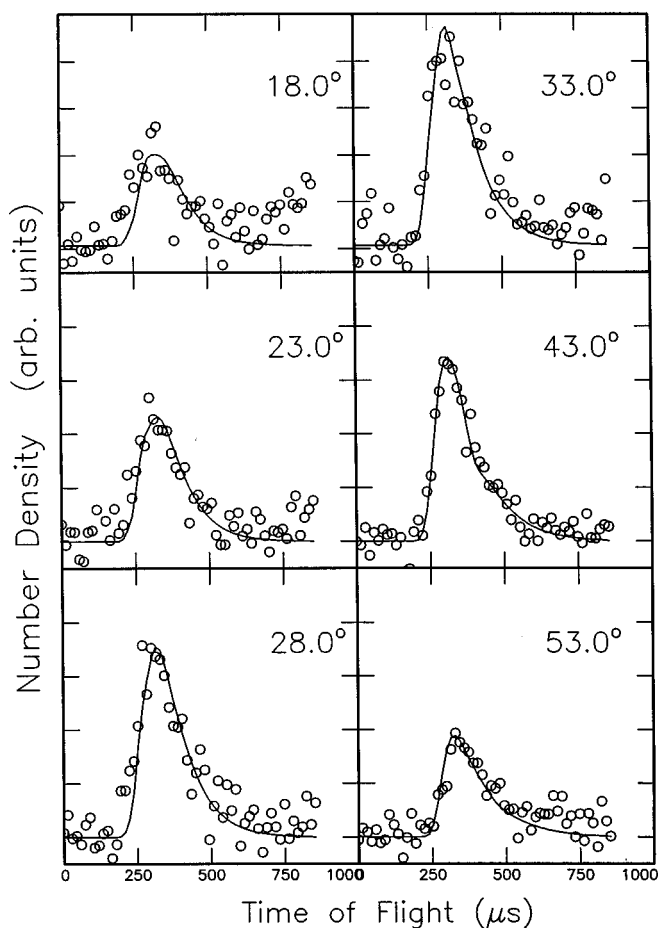


FIG. 7. Time-of-flight data at $m/e=45$ for distinct laboratory angles at a collision energy of 34.9 kJ mol^{-1} . The open circles represent experimental data, and the solid line the fit. The TOF spectra have been normalized to the relative intensity at each angle.

metry as found in earlier experiments²³ and an 1A_1 electronic ground state wave function. Its singlet-triplet gap of $167.5 \text{ kJ mol}^{-1}$ to triplet thioformaldehyde $\{6\}$ (a^3A'') agrees well with recent spectroscopic investigations of 174 kJ mol^{-1} .²⁴ In contrast to previous *ab initio* calculations which predict a planar C_{2v} structure of $\{6\}$,²⁵ the present computations indicate that the two hydrogen atoms are located 20.3° outside the plane (C_s symmetry). Typical carbon-sulfur distances in organic molecules range from 182 to 185 pm (C-S single bond), to 160–165 pm (C=S double bonds), and 150–155 pm (C≡S triple bonds), about 30 pm longer than corresponding carbon-carbon bonds.⁸ Comparing these data with the geometry of $\{7\}$, we find that the carbon-sulfur bond length of 162.2 pm resembles a C=S double bond. Upon singlet-triplet excitation from $\{7\}$ to $\{6\}$, the S-C bond length is elongated by 9.3 pm from 162.2 to 171.5 pm and the SCH angle is reduced by 3.7° from 122.0° to 118.3° . This gives an a^3A'' electronic wave function.

Two other isomers, singlet *trans*- and *cis*-thiohydroxycarbene $\{4\}/\{5\}$, HCSH, have both C_s symmetry and an $^1A'$ electronic ground state wave function. $\{4\}$ and $\{5\}$ lie 184.8 and $189.9 \text{ kJ mol}^{-1}$ above singlet thioformaldehyde. Their carbon-sulfur distances are close to C=S bonds and differ by only 2.1 pm. Triplet thiohydroxycarbene $\{3\}$

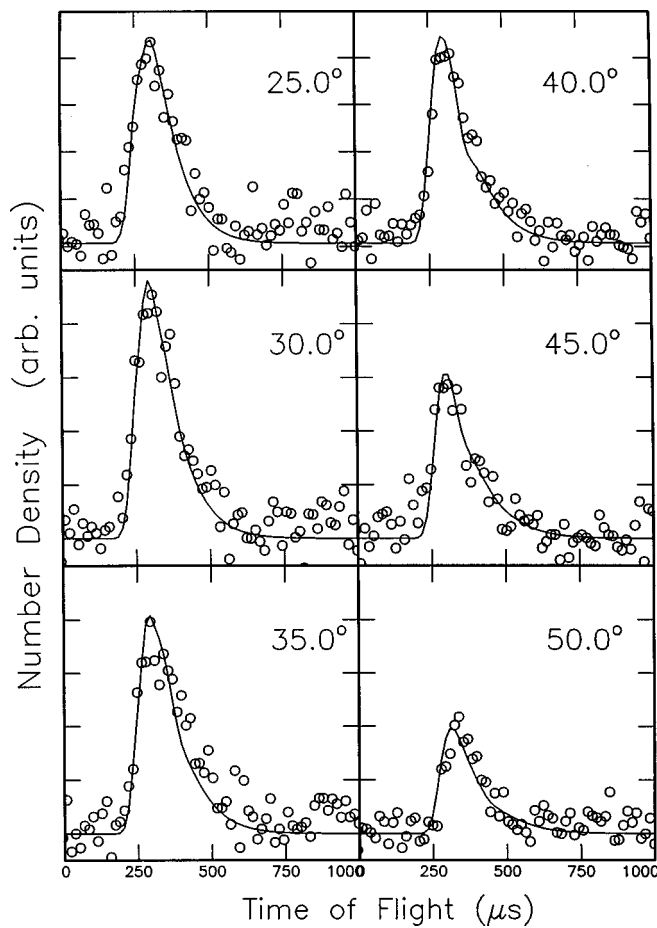


FIG. 8. Time-of-flight data at $m/e=45$ for distinct laboratory angles at a collision energy of 42.8 kJ mol^{-1} . The open circles represent experimental data, and the solid line the fit. The TOF spectra have been normalized to the relative intensity at each angle.

has no symmetry element (C_1 point group, a^3A electronic wave function) and is energetically less favored by 76.1 kJ mol^{-1} compared to singlet *trans*-thiohydroxycarbene. In contrast to $\{4\}$ and $\{5\}$ the carbon-sulfur distance in $\{3\}$ is increased to 171.7 pm, between a carbon-sulfur single and a double bond, and the in-plane C-H bond is rotated out of plane giving the C_1 symmetry of $\{3\}$.

Finally, triplet and singlet 2,2 dihydrothiocarbonyl $\{2\}/\{1\}$, H_2SC , are only 63.5 and 57.3 kJ mol^{-1} more stable than the reactants. The small singlet-triplet splitting of only 6.2 kJ mol^{-1} could facilitate intersystem crossing (ISC). $\{1\}$ belongs to the C_{2v} point group (a^1A_1) and has a typical C=S

TABLE II. Thermochemistry of the reaction $\text{C}(^3P_j) + \text{H}_2\text{S}(X^1A_1)$. The enthalpies of formations of HCS/HSC were taken from our *ab initio* calculations, others from Ref. 21.

Channel	Exit channel	Free reaction enthalpy at 0 K, $\Delta_R H(0 \text{ K}) (\text{kJ mol}^{-1})$
1	$\text{HCS}(X^2A') + \text{H}(^2S_{1/2})$	-183.9
2	$\text{HSC}(X^2A') + \text{H}(^2S_{1/2})$	-18.3
3	$\text{CS}(X^1\Sigma^+) + \text{H}_2(X^1\Sigma_g^+)$	-462.0 ± 2.0
4	$\text{CS}(X^1\Sigma^+) + 2\text{H}(^2S_{1/2})$	-26.0 ± 2.0

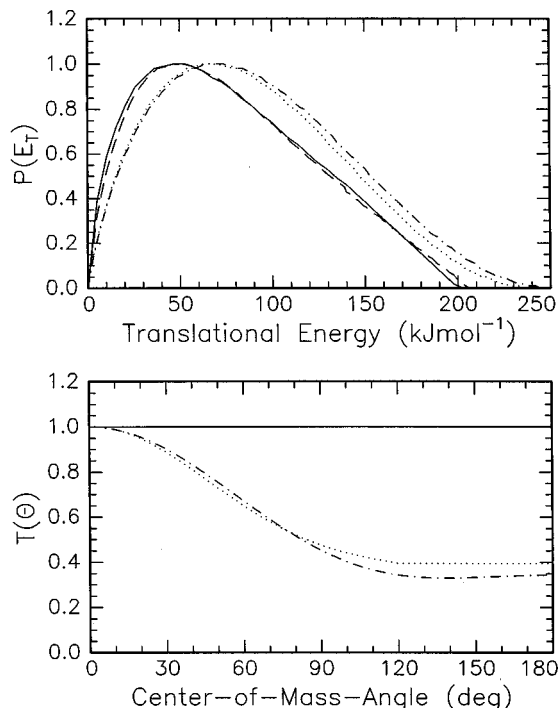


FIG. 9. Bottom: Center-of-mass angular flux distributions for the reaction $C(^3P_j) + H_2S(X^1A_1)$ at collision energies of 16.7 and 20.9 (solid line), 34.9 (dotted), and 42.8 kJ mol^{-1} (dashed-dotted line). Both lower collision energies show an isotropic distribution. Top: Center-of-mass translational energy flux distributions for the reaction $C(^3P_j) + H_2S(X^1A_1)$ at collision energies of 16.7 (solid line), 20.9 (dashed line), 34.9 (dotted line), and 42.8 kJ mol^{-1} (dashed-dotted line).

TABLE III. Maximum impact parameter, b_{max} , maximum initial orbital angular momentum, L_{max} , and capture cross sections σ for four relative collision energies, E_{coll} , employed in our experiments. Cross sections σ are calculated for no [$P(b)=1$], one [$P(b)=2/3$], and two [$P(b)=1/3$] repulsive surfaces of the split triplet manifold.

E_{coll} (kJ mol^{-1})	b_{max} (\AA)	L_{max}, \hbar	σ (\AA^2) [$P(b)=1$]	σ (\AA^2) [$P(b)=2/3$]	σ (\AA^2) [$P(b)=1/3$]
16.7	3.8	102	45	22.5	15
20.9	3.6	109	41	20.5	13.7
34.9	3.3	129	34	17	11.3
42.8	3.2	139	32	16	10.7

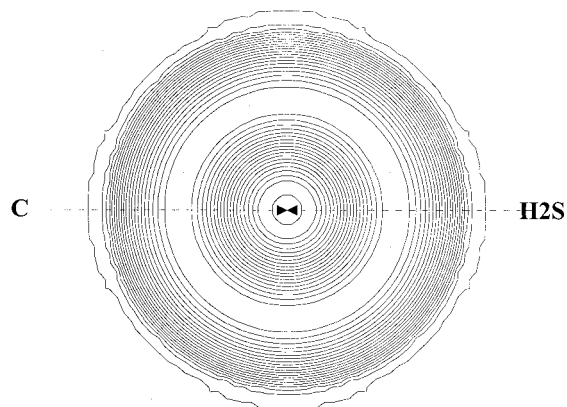


FIG. 11. Contour flux map distribution for the reaction $C(^3P_j) + H_2S(X^1A_1)$ at a collision energy of 20.9 kJ mol^{-1} .

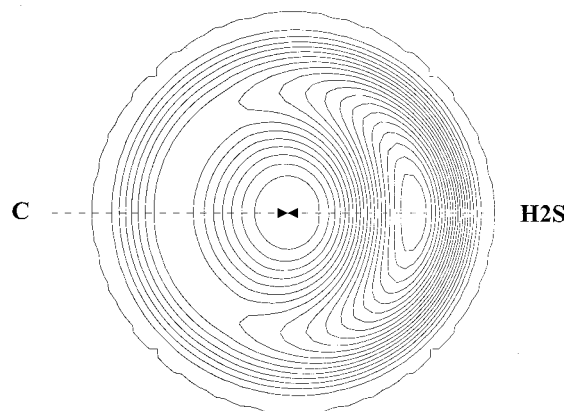


FIG. 12. Contour flux map distribution for the reaction $C(^3P_j) + H_2S(X^1A_1)$ at a collision energy of 34.9 kJ mol^{-1} .

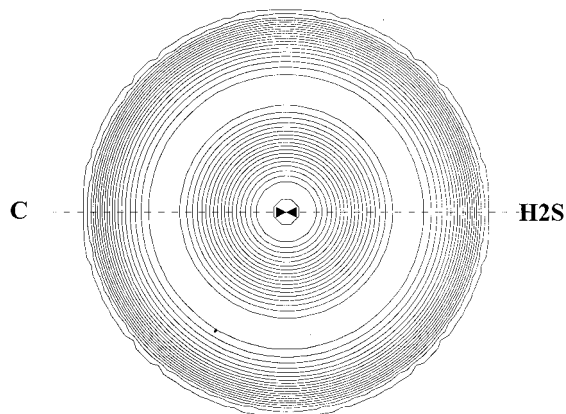


FIG. 10. Contour flux map distribution for the reaction $C(^3P_j) + H_2S(X^1A_1)$ at a collision energy of 16.7 kJ mol^{-1} .

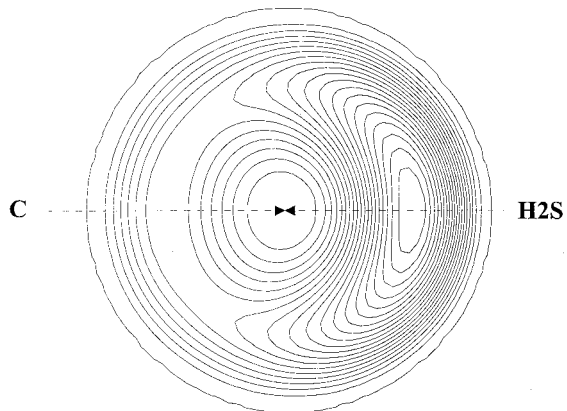


FIG. 13. Contour flux map distribution for the reaction $C(^3P_j) + H_2S(X^1A_1)$ at a collision energy of 42.8 kJ mol^{-1} .

TABLE IV. *Ab initio* equilibrium structures of CH₂S and HCS isomers. The parameters are designated as follows: (S-C) denotes bond length in pm, (S,C,H) the bond angle with an apical atom C(S,H,H,C), the out-of-plane angle between the S-C bond and the H-H-C plane, and (H-C-S-H) the torsion angle H-C-S-H.

Isomer	Structural data
¹ H ₂ CS	(S-C)=162.2; (C-H)=108.8; (S,C,H)=122.0°
³ H ₂ CS	(S-C)=171.5; (C-H)=108.2; (S,C,H)=118.3° (S,H,H,C)=20.3°
¹ HCSH _{trans}	(H-C)=110.8; (C-S)=168.3; (S-H)=135.4; (H,C,S)=100.8°; (C,S,H)=99.6°
¹ HCSH _{cis}	(H-C)=110.0; (C-S)=166.2; (S-H)=137.7; (H,C,S)=109.5°; (C,S,H)=109.4°
³ HCSH	(H-C)=108.4; (C-S)=171.7; (S-H)=135.3 (H,C,S)=129.6°; (C,S,H)=98.5° (H-C-S-H)=97.2°
¹ H ₂ SC	(C-S)=160.8; (S-H)=139.6; (C,S,H)=132.1°
³ H ₂ SC	(C-S)=196.5; (S-H)=135.4; (C,S,H)=104.6° (C,H,H,S)=68.7°
HCS	(H-C)=108.7; (C-S)=156.4; (H,C,S)=132.3°
HSC	(H-S)=136.7; (S-C)=165.6; (H,S,C)=102.7°

double bond distance of 160.8 pm. The triplet isomer {2} depicts a reduced C_s symmetry (X^3A'') and shows the largest carbon-sulfur bond distance of 196.5 pm observed in this study. The S-H bond distance in {2} of 135.4 pm is 1.1 pm longer compared to that of H₂S and the H-S-H bond angle changes only 0.3° from 92.5° in H₂S to 92.2° in {2}. Therefore, we should classify {2} as a van der Waals complex between $C(^3P_j)$ and H₂S rather than covalently bound.

On the HCS/HSC doublet potential energy surface, HSC is less stable by 165.6 kJ mol⁻¹ compared to HCS. Both isomers have C_s symmetry and a $^2A'$ ground state electronic wave function. The HCS enthalpy of formation of 296.2 kJ mol⁻¹ computed²⁶ agrees well with photoionization mass spectrometric studies [300.4 ± 8.4 kJ mol⁻¹ (Ref. 27)] and previous *ab initio* calculations yielding 296.7 kJ mol⁻¹.²⁸ The carbon-sulfur bond in HCS is 5.8 pm shorter compared to singlet thioformaldehyde {7}, thus it ranges between typical C=S and C≡S bond distances. Further, the HCS angle opens up from 122.0° in {7} to 132.3° in HCS. Finally, the reaction exothermicities to form HCS+H and HSC+H are computed to be 183.9 and 18.3 kJ mol⁻¹, respectively.

B. Possible reaction pathway(s) to the HCS isomer

We now outline all theoretically feasible reaction pathways leading to the HCS isomer. In Sec. V C we narrow these possibilities down to those which can account for the shape of the center-of-mass distributions. Addition of $C(^3P_j)$ forms the van der Waals complex {2}, whereas insertion of hydrogen sulfide into the S-H bond might yield triplet thiohydroxycarbene {3}. A hydrogen migration in {2} could lead to {3}, which fragments to HCS and H or rearranges to triplet thioformaldehyde {6}. {6} itself can decompose into the thioformyl radical and atomic hydrogen. Alternatively, {3} or {6} might undergo intersystem crossing to form {4}/{5} or {7}, respectively. Hereafter, {4}/{5} either decompose directly to HCS+H or rearrange to singlet thioformaldehyde {7} prior to fragmentation. Likewise, we should not discard ISC from {6}

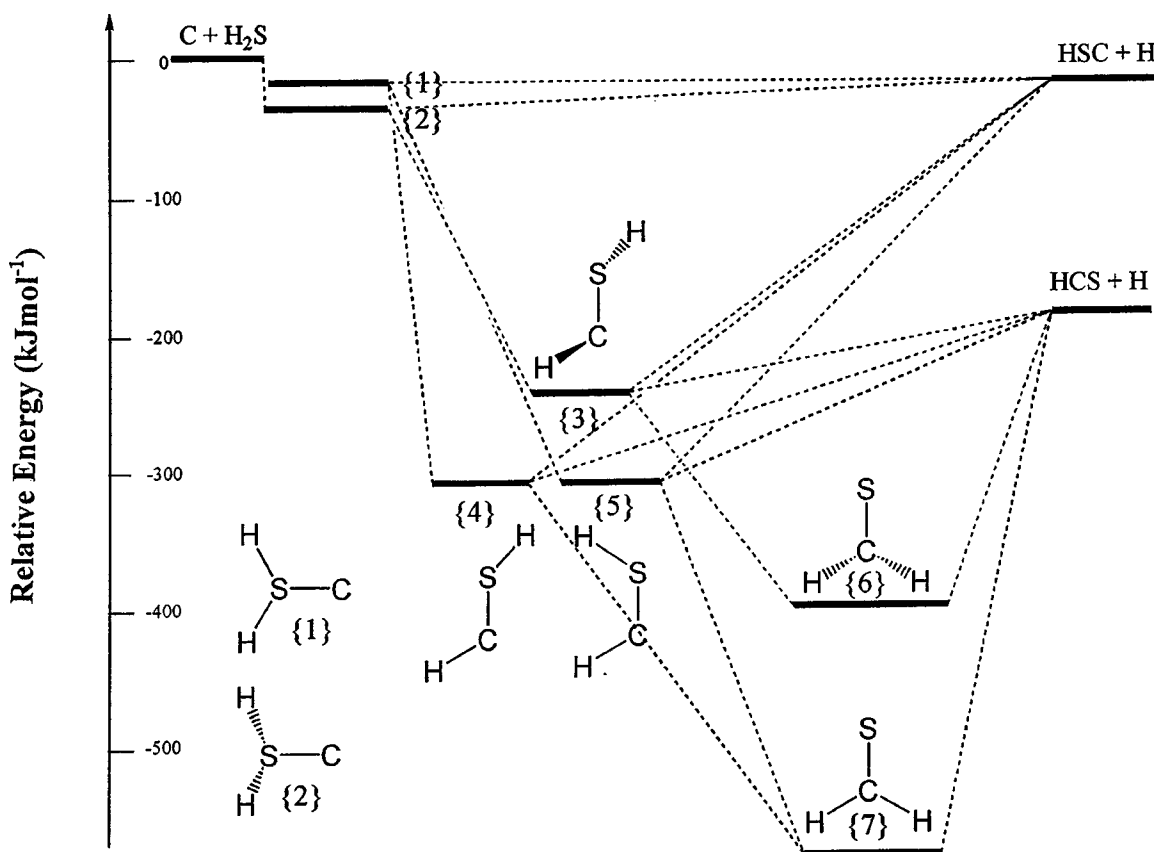


FIG. 14. Schematic representation of the lowest energy pathways on the singlet and triplet CH₂S potential energy surfaces. The bond orders are not included.

to {7} or {2} to {1} as further reaction possibilities. In Sec. VC, we try to exclude some of these possibilities.

C. Rotation axes of decomposing CH₂S complexes

The rotation axes of the CH₂S complexes can help to explain the shape of the $T(\theta)$ distributions and yield further information on the chemical dynamics of the title reaction. Here, we apply the requirement that the carbon atom incorporated and the H atom leaving be placed on different sides of the rotation axis of the fragmenting complex; see Sec. IV D. Based on this, we can eliminate certain reaction pathways discussed in Sec. VB and identify CH₂S complexes which could form the HCS isomer. Since we identified the HCS radical as the major contributor to our reactive scattering signal, neither {1} nor {2} resembles the fragmenting complex. Here, rupturing of a S–H bond would form only the less stable HSC isomer. Based on our *ab initio* calculations, the thioformaldehyde isomers {6} and {7} can be eliminated as well, because the C atom and departing H atom are not placed on the opposite side of the A, B, or C rotational axis. Therefore, the thiohydroxycarbenes {3}, {4}, and {5} are the only remaining candidates. Each of them can rotate around the B/C axis, resulting in a forward peaked $T(\theta)$ and hence HCS and H in the final bond rupture. The exclusion of the A axis is further evidence considering energy and momentum conservation during the reaction. Here, the rotational angular momentum of the decomposing thiohydroxycarbene complex j_{HCSH} equals the initial angular momentum L' . Our *ab initio* rotational constants (Table V) classify {3}–{5} as highly prolate asymmetric tops with asymmetry parameters $\kappa\{3\} = -0.994$, $\kappa\{4\} = -0.980$, and $\kappa\{5\} = -0.981$. Based on these data, we can estimate the energy necessary to excite A-like rotations, E_A , in the symmetric top approximation taking the rotational quantum number j_{HCSH} from $L = j_{\text{HCSH}}\hbar$. This procedure yields $E_A = 7751 - 16890 \text{ kJ mol}^{-1}$. Even assuming a maximum available energy of $408.4 \text{ kJ mol}^{-1}$ to form {4}, less than 5% of the thiohydroxycarbene intermediates are in an A rotational state even if all the reactions proceed with a maximum impact parameter b_{max} . Hence, an A rotational axis of {3}–{5} is expected to play only a minor role in the chemical dynamics in forming the HCS isomer. Further, neither B nor C, like rotational excitations in the thiohydroxycarbene, can interconvert both H atoms, and the symmetric center-of-mass angular distributions at both lower collision energies are the result of a decomposing complex with a lifetime that is longer than its rotational period.

Finally, we compare the addition pathway to yield {2} to the insertion pathway giving {3}. The formation of a van der Waals complex requires basically no entrance barrier, only the centrifugal barrier. $C(^3P_j)$ insertion into the S–H bond of H₂S to {3} is likely to produce a significant entrance barrier, one much larger than our lowest collision energy since this reaction is symmetry forbidden. The slight negative energy dependence, i.e., an increasing cross section as the collision energy is lowered, suggests that the large impact parameters b dominate the opacity function. However, trajectories with small impact parameters of less than about

200 pm prefer the insertion process, whereas our calculations show b values up to 390 pm could lead to the reactive scattering signal. Since H₂S holds a H–S–H angle of only 92.5°, the nonbonding b_1 and $2a_1$ orbitals of hydrogen sulfide have a high p -orbital character.²⁹ Compared to the H–S– σ orbitals, the p -electron density extends to larger radii, thus increasing the cone of acceptance in contrast to approach geometries toward the S–H– σ bond. Therefore, an addition pathway to {2} is the first step of the reaction likely, followed an ISC to {1} or by hydrogen migration to {3}. {3} could undergo ISC to {4}/{5} prior to final bond rupture to form a HCS radical excited to B or/and C like rotations. These rotations account for the forward peaked center-of-mass angular distributions at higher collision energies. At both lower collision energies, the isotropic $T(\theta)$ cannot exclude a decomposing thioformaldehyde complex.

D. Approach geometries of C(³P_j) towards H₂S

We now discuss distinct approach geometries of the carbon atom toward the hydrogen sulfide molecule. Although the crossed beam experiments cannot give an explicit answer as to which trajectory is preferred, the following helps one to understand the trajectory-dependent rotational excitation of the reactive intermediates. First, the electrophile carbon atom could initially approach with its empty p_x orbital (a_1 symmetry) toward the nonbonding a_1 orbital at the sulfur atom in the HHSC plane (C_{2v} approach, a head on collision with $b = 0$ impact parameter), see Fig. 15(a). As $C(^3P_j)$ advances closer, both H atoms are bent out of the HHCS plane to form {2}. This excites rotations around the B axis located roughly perpendicular to the original m_2 plane. Since the C_{2v} symmetry is reduced to C_s , this approach geometry proceeds on the ³A' surface. Alternatively, carbon atoms might approach under C_s symmetry within the m plane either parallel to the HSH molecular or perpendicular to this plane. These limiting cases are shown in Figs. 15(b) and 15(c), respectively. In both scenarios, the empty p_y orbital (b_1 symmetry) located at the carbon atom interacts preferentially with the nonbonding b_1 orbital of the S atom. These trajectories could preserve C_s symmetry, proceed on the ³A' surface, open larger impact parameters compared to the case in Fig. 15(a), and excite B like rotations of the H₂SC van der Waals complex, Fig. 16. In addition, $C(^3P_j)$ can attack within the SHS molecular plane; see Figs. 15(d) and 15(e). In both cases, the empty p_x orbital at the C atom (a_1 symmetry) interacts with the nonbonding a_1 orbital at the sulfur atom. Since both H atoms bend out of the plane, these pathways follow the ³A surface (C_1 symmetry) and can excite C like rotations of the triplet CH₂S. Compared to the cases of Figs. 15(a)–15(c), however, the overlap of the nonbonding orbital located at the S atom with the empty p orbital of the carbon atom is expected to be smaller and hence the attractive long-range potential weaker. Therefore, these trajectories should contribute to a lesser extent to form triplet CSH₂. Finally, an out-of-plane approach (C_1 symmetry) can lead to B/C like rotations.

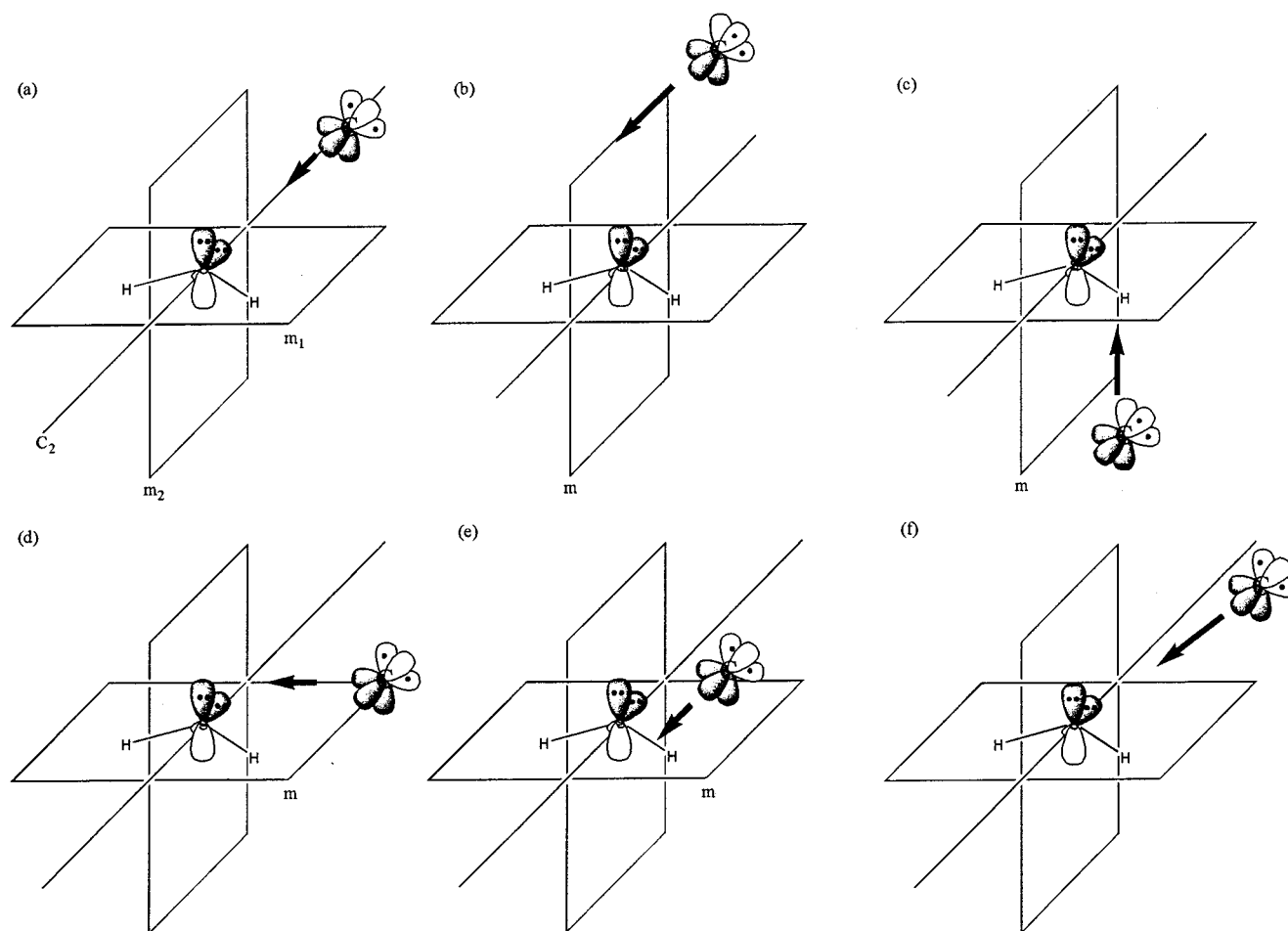


FIG. 15. Approach geometries of the carbon atom towards the hydrogen sulfide molecule (see the text for details). The bold face arrows indicate the approach geometry. Double dots symbolize nonbonding orbitals at the sulfur atom, and single dots singly occupied p orbitals of the approaching carbon atom. The doubly occupied $2s$ orbital of the C atom is not shown.

E. Lifetime of thiohydrocarbene complexes

Having narrowed the decomposing complexes to thiohydrocarbenes {3}, {4}, and/or {5}, we can estimate their lifetimes $\tau(i)$ in a complex rotating around its i axis. The oscillating complex model relates τ to the intensity ratio of $T(\theta)$ at 0° and 180° . If we employ the rotational constants from our *ab initio* calculations, we estimate $\tau(A) = 0.01\text{--}0.007$ ps and $\tau(B/C) = 0.118\text{--}0.082$ ps, see Table V. Reactions involving short-lived intermediates with lifetimes <0.1 ps follow direct scattering dynamics.³⁰ In this case, the $T(\theta)$'s should be strongly forward scattered and are expected to show less intensity at backward angles, as was

TABLE V. Rotational constants (in cm^{-1}) and lifetime τ (in ps) of HCSH complexes calculated for rotations about the A, B and C axes at collision energies of 34.9 and 42.8 kJ mol^{-1} .

Isomer	A	B	C	34.9 kJ mol^{-1}			42.8 kJ mol^{-1}		
				$\tau(A)$	$\tau(B)$	$\tau(C)$	$\tau(A)$	$\tau(B)$	$\tau(C)$
¹ HCSH _{trans}	6.164	0.613	0.558	0.011	0.103	0.111	0.008	0.082	0.091
¹ HCSH _{cis}	6.347	0.615	0.560	0.009	0.102	0.112	0.008	0.082	0.091
³ HCSH	7.251	0.550	0.530	0.008	0.114	0.118	0.007	0.096	0.117

found experimentally. Comparing the order of magnitude of this lifetime with those estimated from our $T(\theta)$'s, we find that HCSH molecules rotating around the A axis are not decomposing complexes. This finding is in line with the distinct accessible rotational axis; cf. Sec. V C. Hence HCSH as well as the HCS product are excited to B/C like rotations.

F. Upper, average limit of the exit impact parameter b'

The total available energy, E_{tot} , of the reaction channels into product translation, E_{tr} , rotation, E_{rot} , and vibration, E_{vib} . E_{tr} can be approximated from the $P(E_T)$'s as the average translational energy releases $\langle E_T \rangle$. If we assume no vibrational excitation of the HCS product, we can estimate a maximum of E_{rot} and an upper limit of the rotational quantum number J . Then the final j' rotational angular momentum can be calculated. Due to total angular momentum conservation, this leads to a lower limit of the final orbital angular momentum L' . Keeping in mind that $L' = \mu' \times v_r' \times b'$ with the reduced mass of the products μ' , the relative velocity v_r' , and the exit impact parameter b' , we can estimate an upper, averaged limit of the exit impact parameter b' within the orbiting limit approximation. Specifically, the

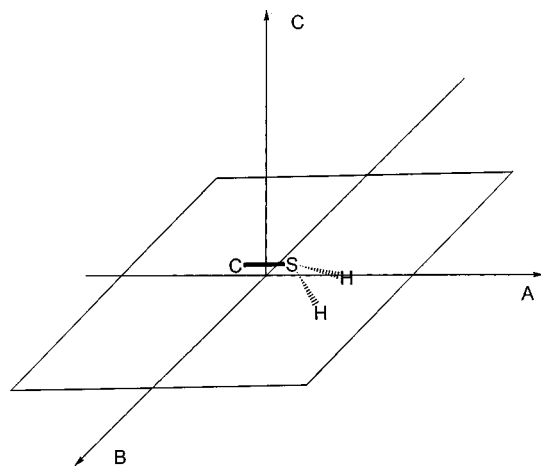


FIG. 16. Schematic representation of A, B, and C rotational axes in the triplet CSH₂ van der Waals complex.

average maximum available energies channeling into rotation are calculated to be $E_{\text{rot}} = 123.6 \text{ kJ mol}^{-1}$ ($E_{\text{coll}} = 16.7 \text{ kJ mol}^{-1}$), $125.8 \text{ kJ mol}^{-1}$ ($E_{\text{coll}} = 20.9 \text{ kJ mol}^{-1}$), $129.8 \text{ kJ mol}^{-1}$ ($E_{\text{coll}} = 34.9 \text{ kJ mol}^{-1}$), and $134.7 \text{ kJ mol}^{-1}$ ($E_{\text{coll}} = 42.8 \text{ kJ mol}^{-1}$); cf. Sec. IV C. The rotational constants of HCS, i.e., $A = 30.783 \text{ cm}^{-1}$, $B = 0.678 \text{ cm}^{-1}$, and $C = 0.663 \text{ cm}^{-1}$,¹⁸ classify this radical as a highly prolate asymmetric top with asymmetry parameter $\kappa = -0.9990$. Due to the large A rotational constant, the rotational level $K_a = 0$ is well separated from other K_a levels, and we can simplify the treatment as if HCS were a linear molecule with $K_a = 0$. An upper limit of J calculates via $E_{\text{rot}} = hcBJ(J+1)$. This yields upper limits of j' of about $45\hbar$, and L' is about $60\hbar$ ($E_{\text{coll}} = 16.7 \text{ kJ mol}^{-1}$), $67\hbar$ ($E_{\text{coll}} = 20.9 \text{ kJ mol}^{-1}$), $87\hbar$ ($E_{\text{coll}} = 34.9 \text{ kJ mol}^{-1}$), and $97\hbar$ ($E_{\text{coll}} = 42.8 \text{ kJ mol}^{-1}$). Based on these data, we calculate exit the impact parameters b' to be $< 670 \text{ pm}$ (Fig. 16).

G. Exit transition state

The collision energy dependent shape of the $P(E_T)$'s together with the average translational energy releases, $\langle E_T \rangle$, expose aspects of the dynamics between the formation of the thiohydroxycarbene complex(es) and the final fragmentation to HCS+H. At lower collision energies both $P(E_T)$'s peak at 44–53 kJ mol^{-1} , whereas the distribution maximum is shifted towards higher energies of 61–72 kJ mol^{-1} as the collision energy rises to 34.9 and 42.8 kJ mol^{-1} . This suggests that final S–H bond rupture involves a tight exit transition state located about 44–72 kJ mol^{-1} above the products. The principle of microscopic reversibility dictates that the reversed reaction of atomic hydrogen with the HCS(X^2A') radical has an identical entrance barrier height. But this order of magnitude seems quite surprising since atom-radical reactions are thought to resemble barrierless reactions if their radical centers recombine. A better picture is obtained if we compare the structural geometries of the thiohydroxycarbene complexes with the HCS product cf. Table IV. The most significant change is the shorter carbon–sulfur bond from 166.2–171.7 to 156.4 pm in HCS. This resembles a transition from a C=S double to a C≡S triple bond.

Hence the reversed reaction likely involves a hydrogen atom attacking the triple bond rather than a free radical center.

H. Comparison with the reaction $O(^3P_j/{}^1D_2) + H_2S$

The chemical dynamics of the $O(^3P_j/{}^1D_2)/H_2S$ system were studied recently by Alagia *et al.*³¹ in crossed molecular beam experiments at collision energies between 14.2 and 49.4 kJ mol^{-1} . The reaction of $O(^1D_2)$ is found to proceed via its insertion into the S–H bond through a long-lived singlet HSOH complex that decomposes into HSO and a H atom. As the collision energy rises, the lifetime of the intermediate is reduced to less than a rotational period, hence the chemical dynamics follow those of an osculating complex. $O(^3P_j)$ however, shows direct rebound scattering dynamics, and the flux contour map shows only intensity in the backward direction with respect to the oxygen beam. Compared to our reaction, the difference in the chemical dynamics is likely based on the existence/nonexistence of a triplet addition complex formed from the reactants. *Ab initio* calculations of the triplet OH₂S potential energy surface depict no bound OSH₂ intermediate,³² and no rearrangement to a long-lived HOSH complex can take place. In fact, all triplet the OSH₂ structures are transition states to form HSO+H products. This results in direct scattering dynamics of the $O(^3P_j)/H_2S$ system without complex formation and could explain further the inhibited formation of the SOH isomer which is only 3–4 kJ mol^{-1} less stable compared to its HSO counterpart.

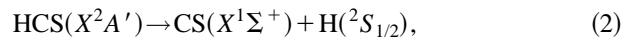
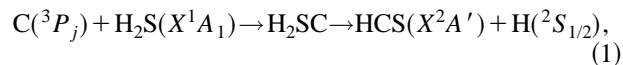
I. The undetected HSC isomer

Our present investigations show that the thermodynamically less stable HSC isomer is formed to less than 10%. This might indicate that the barrier of H atom elimination from the initially formed triplet CSH₂ complex is much larger than the barrier for the H atom migration to triplet thiohydroxycarbene. Further, the C–H bond strengths in the thiohydroxycarbene complexes are 120–180 kJ mol^{-1} stronger compared to these of S–H bonds,⁸ and the latter are cleaved preferentially. Preliminary experiments on $C(^1D_2)$ with acetylene and propylene show that the reactions follow direct abstraction dynamics.³³ The scattering signal is confined solely to the forward sphere with respect to the carbon beam indicating that the reaction proceeds either from the reactants to the products through only one transition state or that the intermediate involved is extremely short lived. If we apply these findings, a reaction of $C(^1D_2)$ with H₂S might proceed via a very short-lived singlet CSH₂ intermediate decomposing and forming HSC+H.

VI. COMBUSTION CHEMISTRY IMPLICATIONS

The HCS radical identified in our studies might represent the missing link between sulfur containing molecules in coal and sulfur containing polycyclic aromatic hydrocarbons formed in the combustion of sulfur containing fuel. In this process H₂S can be transformed into highly unstable thioformyl intermediate HCS, which can decompose into H atoms and extremely reactive CS. The latter was detected in hydrocarbon flames,⁶ but its source has not yet been re-

solved. The open shell species HCS is expected to react with atomic oxygen without an entrance barrier with rate constants of the order of $10^{-10} \text{ cm}^3 \text{ s}^{-1}$, possibly transforming HCS into the OCS detected in combustion processes. Hence, the role of reactions (1)–(3),



should be investigated in future combustion flame models.

VII. SOLAR SYSTEM APPLICATIONS

Our results are useful to unravel the complex impact induced chemistry during collision of SL9 with Jupiter.³⁴ We identified the thioformyl radical, HCS, as the major product of $\text{C} + \text{H}_2\text{S}$ under single collision laboratory conditions. This reaction could account for the unassigned HCS source required for chemical reaction networks to match the observed CS abundance in the impact plumes from the collision of SL9 fragments into Jupiter. At 5000 K, chemical models predict atomic carbon to be present during the initial impact,³⁵ and the most probable translation energy is about 50 kJ mol^{-1} which is close to our collision energy of 42.4 kJ mol^{-1} . The high-energy tail of the Maxwell-Boltzman distribution could enable HCS to be formed with more internal energy so that it undergoes a secondary decomposition into CS and H in the jovian atmosphere. Further, our experiments classify a thiohydroxycarbene complex, HCSH, as the reaction intermediate to form HCS and H. Although its lifetime is too low for it to survive in our experiments, the denser jovian atmosphere could supply a three body collision. In this way internal energy can be diverted, thus stabilizing the HCSH intermediate. HCSH should be included in future models of impact induced chemistry of SL9 into Jupiter.

VIII. ASTROPHYSICAL IMPLICATIONS

The formation of the thioformyl radical, $\text{HCS}(X^2A')$, via the atom–neutral reaction of $\text{C}(^3P_j)$ with H_2S might help unravel the chemistry in dark clouds and in circumstellar envelopes of old carbon stars. H_2S is ubiquitous in the interstellar medium (ISM) and has been observed, for example, in molecular clouds TMC-1 and OMC-1, toward the star forming region SgrB2, and around the circumstellar envelope of the carbon star IRC+10216.^{36,37} Upon reaction of $\text{C}(^3P_j)$ with hydrogen sulfide, a C–S bond can be formed in the gas phase. Subsequently, HCS could react with C, N, or even O atoms to yield C_2S , NCS, or OCS; see Fig. 17. This reaction chain involves two successive carbon attacks and could explain the formation of $\text{C}_2\text{S}/\text{C}_3\text{S}$ detected in the envelope surrounding the carbon star IRC+10216,³⁸ or C_2S observed in the dark cloud TMC-1.³⁹ This channel represents an alternative to hitherto postulated ion-molecule reactions involving S atoms and hydrocarbon ions contributing to C_2S and C_3S .^{40,41} Very recently Yamamoto and co-workers detected microwave transitions of the HCS radical in terrestrial labs.⁴² These data are useful to search for the HCS intermediate in

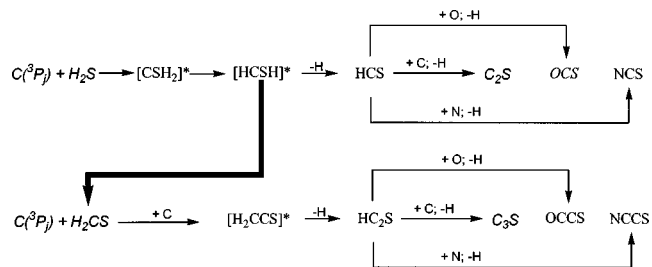


FIG. 17. Schematic reaction pathways to form carbon–sulfur containing molecules in the interstellar medium. Species in italics have been observed in the interstellar medium. The bold face arrows depict reaction pathways through phonon interactions that are only feasible on interstellar grains.

the neighborhood of dark clouds and circumstellar envelopes where $\text{C}(^3P_j)$, H_2S , as well as C_2S have been detected. Once a systematic correlation of these species is established, refined reaction networks of these environments could test the influence of these reactions to the organo-sulfur chemistry.

Complementary to interstellar gas phase chemistry, the dynamics of the title reaction could have an impact on solid state chemistry in icy mantles condensed on interstellar grains. Here, solid H_2S is thought to be formed on/in icy mantles of interstellar grains that have been detected towards W33A.⁴³ Upon reaction of $\text{C}(^3P_j)$ to HCSH via CSH_2 , a H atom migration could yield internally excited thioformaldehyde which might be stabilized on interstellar grains through phonon interaction with the surrounding matrix. Successive heating of these grains by embedded newly formed stars could release H_2S and H_2CS molecules into the gas phase as is documented in distinct *ortho* to *para* spin populations of 1.8 in thioformaldehyde.⁴⁴ This reaction pathway may resolve the anticorrelation of H_2CS and H_2S in carbon rich dark clouds, e.g., in TMC-1, and it may present an alternative method by which to form thioformaldehyde via $\text{S} + \text{CH}_3$. Likewise, thioformaldehyde could react with atomic carbon to produce $\text{HC}_2\text{S} + \text{H}$. Upon attack of a second carbon atom a reaction to C_3S occurs. Finally, formation of HCS on interstellar grains and the subsequent reaction with atomic oxygen to form solid COS could replace the hitherto assumed pathway involving the reaction $\text{O}(^3P_j) + \text{H}_2\text{S}$. At 10 K, the entrance barrier of the latter reaction cannot be overcome.⁴⁵

IX. CONCLUSIONS

The reaction between ground state carbon atoms, $\text{C}(^3P_j)$, and hydrogen sulfide, $\text{H}_2\text{S}(X^1A_1)$, was studied at four average collision energies between 16.7 and 42.8 kJ mol^{-1} using the crossed molecular beam technique. Reaction dynamics inferred from the TOF spectra and LAB distributions were combined with *ab initio* calculations and suggest that the reaction proceeds through an addition of $\text{C}(^3P_j)$ to the sulfur atom that forms a triplet CSH_2 van der Waals complex, followed by H atom migration on the singlet/triplet surface to form a thiohydroxycarbene intermediate HCSH rotating around the *B/C* axis. HCSH decomposes through a tight exit transition state into atomic hydrogen and HCS in its $^2A'$ electronic ground state. At lower collision energies, a weak *L–L'* correlation leads to isotropic center-of-mass angular distributions. As the collision energy rises, the distri-

butions show a pronounced forward scattering, documenting the reaction involves an osculating complex. The identification of HCS under single collision conditions is a one-step pathway which could form a carbon–sulfur bond in combustion processes, interstellar environments, and the collision of comet Shoemaker-Levy 9 with Jupiter. However, much work remains to be done. Transition state calculations are necessary to investigate the mechanism further. First, the barriers for H atom migration from $\{1\}/\{2\}$ to $\{3\}/\{4\}/\{5\}$ and the possible insertion of the carbon atom remain to be investigated theoretically. Second, the decomposing HCSH complex(es) must be identified. Finally, ISC rate constants might help to unravel the role of the singlet PES and hence that of intermediates $\{1\}$, $\{4\}$, and/or $\{5\}$.

ACKNOWLEDGMENTS

Two of the authors (R.I.K. and C.O.) thank the Deutsche Forschungsgemeinschaft (DFG) for Habilitation and post-doctoral fellowships, respectively. One of the same authors (R.I.K.) acknowledges support by Professor D. Gerlich (TU Chemnitz, Germany). Thanks to Dr. I. Hahndorf of the Institute of Atomic and Molecular Sciences, Academia Sinica, (IAMS) for comments on the manuscript. One author (M.H.G.) acknowledges a Packard fellowship. This work was supported by the Director, Office of Energy Research, Office of Basic Energy Sciences, Chemical Sciences Division of the U.S. Department of Energy under Contract No. DE-AC03-76SF00098.

- ¹H. Scheffler and H. Elsässer, *Physics of the Galaxy and Interstellar Matter* (Springer, Berlin, 1988).
- ²D. J. Hollenbach and H. A. Thronson, *Interstellar Processes* (Reidel, Dordrecht, 1987).
- ³E. L. O. Bakes, *The Astrochemical Evolution of the Interstellar Medium* (Twin, Vledder, 1997).
- ⁴P. Eberhard, R. Meier, D. Krankowsky, and R. R. Hodges, *Astron. Astrophys.* **288**, 315 (1994); M. L. Marconi, D. A. Mendis, D. L. Mitchell, R. P. Lin, A. Korth, and H. Reme, *Astrophys. J.* **378**, 756 (1991).
- ⁵*The Collision of Comet Shoemaker-Levy 9 and Jupiter*, edited by K. S. Noll, H. A. Weaver, and P. D. Feldman, (Cambridge University Press, Cambridge, 1996).
- ⁶J. M. Jones *et al.*, *Carbon* **33**, 833 (1995).
- ⁷J. Le Bourlot, G. P. des Forets, E. Roueff, and P. Schilke, *Astrophys. J.* **416**, L87 (1993).
- ⁸*Handbook of Chemistry and Physics* (Chemical Rubber, Boca Raton, FL, 1995).
- ⁹R. I. Kaiser, W. Sun, and A. G. Suits, *J. Chem. Phys.* **106**, 5288 (1997).
- ¹⁰Y. T. Lee, J. D. McDonald, P. R. LeBreton, and D. R. Herschbach, *Rev. Sci. Instrum.* **40**, 1402 (1969).
- ¹¹R. I. Kaiser and A. G. Suits, *Rev. Sci. Instrum.* **66**, 5405 (1995).
- ¹²G. O. Brink, *Rev. Sci. Instrum.* **37**, 857 (1966); N. R. Daly, *ibid.* **31**, 264 (1960).
- ¹³R. J. Buss, Ph.D. thesis, University of California, Berkeley, 1979.

- ¹⁴K. Raghavachari, G. W. Trucks, J. A. Pople, and M. Head-Gordon, *Chem. Phys. Lett.* **157**, 479 (1989); J. D. Watts, J. Gauss, and R. J. Bartlett, *ibid.* **200**, 1 (1992).
- ¹⁵J. F. Stanton, J. Gauss, J. D. Watts, W. J. Lauderdale, and R. J. Bartlett, *Int. J. Quantum Chem., Symp.* **26**, 879 (1992).
- ¹⁶A. Schäfer, H. Horn, and R. Ahlrichs, *J. Chem. Phys.* **97**, 2571 (1992).
- ¹⁷T. H. Dunning, *J. Chem. Phys.* **90**, 1007 (1989).
- ¹⁸C. Ochsenfeld, R. I. Kaiser, Y. T. Lee, and M. Head-Gordon (unpublished).
- ¹⁹R. I. Kaiser, D. Stranges, Y. T. Lee, and A. G. Suits, *J. Chem. Phys.* **105**, 8705 (1996); R. I. Kaiser, D. Stranges, H. M. Bevsek, Y. T. Lee, and A. G. Suits, *ibid.* **106**, 4945 (1997).
- ²⁰W. B. Miller, S. A. Safron, and D. R. Herschbach, *Discuss. Faraday Soc.* **44**, 108 (1967); **44**, 291 (1967).
- ²¹J. O. Hirschfelder, C. F. Curtiss, and R. B. Bird, *Molecular Theory of Gases and Liquids* (Wiley, New York, 1954).
- ²²R. I. Kaiser, C. Ochsenfeld, M. Head-Gordon, Y. T. Lee, and A. G. Suits, *Science* **274**, 1508 (1996); R. I. Kaiser, Y. T. Lee, and A. G. Suits, *J. Chem. Phys.* **105**, 8705 (1996); R. I. Kaiser, D. Stranges, Y. T. Lee, and A. G. Suits, *ibid.* **105**, 8721 (1996).
- ²³M. R. J. Hachey and F. Grein, *J. Mol. Spectrosc.* **172**, 384 (1995).
- ²⁴R. H. Judge, D. C. Moule, and G. W. King, *J. Mol. Spectrosc.* **81**, 37 (1980); M. R. J. Hachey and F. Grein, *Chem. Phys.* **197**, 61 (1995).
- ²⁵M. R. J. Hachey and F. Grein, *Chem. Phys.* **197**, 61 (1995).
- ²⁶The enthalpies of formation $\Delta H_f^0(\text{HCS})$ are calculated via $\Delta H_R^0 = \Delta H_f^0(\text{HCS}) + \Delta H_f^0(\text{H}) - \Delta H_f^0(\text{H}_2\text{S}) - \Delta H_f^0(\text{C})$. Here, ΔH_f^0 was taken from our *ab initio* calculations, $\Delta H_f^0(\text{H})$, $\Delta H_f^0(\text{H}_2\text{S})$, and $\Delta H_f^0(\text{C})$, that were taken from Ref. 21.
- ²⁷B. Ruscic and J. Berkowitz, *J. Chem. Phys.* **98**, 2568 (1993).
- ²⁸L. A. Curtiss, R. H. Nobes, J. A. Pople, and L. Radom, *J. Chem. Phys.* **97**, 6766 (1992).
- ²⁹T. A. Albright, J. K. Burdett, and M. H. Whangbo, *Orbital Interactions in Chemistry* (Wiley, New York, 1985).
- ³⁰R. D. Levine and R. B. Bernstein, *Molecular Reaction Dynamics and Chemical Reactivity* (Oxford University Press, Oxford, 1992).
- ³¹M. Alagia, N. Balucani, P. Casavecchia, D. Stranges, and G. G. Volpi, *J. Chem. Soc., Faraday Trans.* **91**, 575 (1995).
- ³²A. Goumri *et al.*, *J. Chem. Phys.* **102**, 161 (1995); **101**, 9405 (1994).
- ³³R. I. Kaiser and Y. T. Lee (unpublished).
- ³⁴R. I. Kaiser, C. Ochsenfeld, M. Head-Gordon, and Y. T. Lee, *Science* **279**, 1181 (1998).
- ³⁵S. Borunov, P. Drossart, T. Encrenaz, and V. Dorofeeva, *Icarus* **125**, 121 (1997).
- ³⁶P. Thaddeus *et al.*, *Astrophys. J.* **176**, 73 (1997).
- ³⁷Y. C. Minh, L. M. Ziurys, W. M. Irvine, and D. McGonagle, *Astrophys. J.* **366**, 192 (1991).
- ³⁸J. Cernicharo, M. Guelin, H. Hein, and C. Kahane, *Astron. Astrophys. Lett.* **181**, 9 (1987).
- ³⁹H. Suzuki *et al.*, *Astrophys. J.* **392**, 551 (1992).
- ⁴⁰D. A. Rowe and T. J. Millar, *Mon. Not. R. Astron. Soc.* **244**, 444 (1990).
- ⁴¹T. J. Millar and E. Herbst, *Astron. Astrophys.* **231**, 466 (1990).
- ⁴²H. Habara, S. Yamamoto, C. Ochsenfeld, M. Head-Gordon, R. I. Kaiser, and Y. T. Lee, *J. Chem. Phys.* (submitted).
- ⁴³T. R. Geballe, F. Baas, J. M. Greenberg, and W. Schutte, *Astron. Astrophys. Lett.* **432**, L6 (1985).
- ⁴⁴Y. C. Minh, W. M. Irvine, and M. K. Brewer, *Astron. Astrophys.* **244**, 181 (1991).
- ⁴⁵M. E. Palumbo, T. R. Geballe, and A. G. G. M. Tielens, *Astrophys. J.* **479**, 839 (1997).